Journal Pre-proofs

Structural modifications of indolinones bearing a pyrrole moiety and discovery of a multi-kinase inhibitor with potent antitumor activity

Mingze Qin, Ye Tian, Xiao Han, Qi Cao, Shuaishuai Zheng, Chunyang Liu, Xia Wu, Lei Liu, Yangyang Meng, Xiaobo Wang, Haotian Zhang, Yunlei Hou

PII: S0968-0896(20)30307-2
DOI: https://doi.org/10.1016/j.bmc.2020.115486
Reference: BMC 115486

To appear in: *Bioorganic & Medicinal Chemistry*

Received Date: 26 January 2020
Revised Date: 20 March 2020
Accepted Date: 30 March 2020

Please cite this article as: Qin, M., Tian, Y., Han, X., Cao, Q., Zheng, S., Liu, C., Wu, X., Liu, L., Meng, Y., Wang, X., Zhang, H., Hou, Y., Structural modifications of indolinones bearing a pyrrole moiety and discovery of a multi-kinase inhibitor with potent antitumor activity, *Bioorganic & Medicinal Chemistry* (2020), doi: https://doi.org/10.1016/j.bmc.2020.115486

Structural modifications of indolinones bearing a pyrrole moiety and discovery of a multi-kinase inhibitor with potent antitumor activity

Mingze Qin [a,d], Ye Tian [a], Xiao Han [b], Qi Cao [a], Shuaishuai Zheng [a], Chunyang Liu [a], Xia Wu [a], Lei Liu [a], Yangyang Meng [a], Xiaobo Wang [d,*], Haotian Zhang [c,*], Yunlei Hou [a,*]

[a] Key Laboratory of Structure-Based Drug Design and Discovery, Ministry of Education, Shenyang Pharmaceutical University, Shenyang 110016, PR China
[b] School of Pharmacy, Shenyang Pharmaceutical University, Shenyang 110016, PR China
[c] Department of Pharmacology, Shenyang Pharmaceutical University, Shenyang 110016, PR China
[d] Chinese People's Liberation Army Logistics Support Force No. 967 Hospital, Dalian 116021, PR China

*Corresponding authors.
Tel: +86 24 2398 6282
E-mail address: houyunlei901202@163.com (Y. Hou); zhanghaotian2087@163.com (H. Zhang); wxbbenson0653@sina.com (X. Wang).

Abstract

Structural modifications of compound **2**, an angiokinase inhibitor reported by our group were performed, which led to the discovery of methyl (*Z*)-3-(((4-(2-methyl-5-((4-methylpiperazin-1-yl)methyl)-1*H*-pyrrol-1-yl)phenyl)amino)(phenyl)methylene)-2-oxoindoline-6-carboxylate (**7h**). Compound **7h** exhibited excellent inhibitory activity against angiokinases including VEGFR-1/2/3, PDGFRα/β, and FGFR-1, as well as LYN and c-KIT kinases. At the cellular level, compound **7h** significantly attenuated phosphorylation of AKT and ERK proteins, potently inhibited colony formation of HT-29, MKN74, and HepG2 cancer cells, and induced cell apoptosis. Upon incubation with human liver microsome, **7h** exhibited comparable metabolic stability to nintedanib. Compound **7h** has emerged as a promising lead compound for future drug design.

Keywords: structural modification; multi-kinase inhibitor; antitumor activity

1. Introduction

Angiogenesis is an indispensable physiological process during embryonic development and wound healing.[1–3] However, considerable studies demonstrated that the progression of primary tumor is angiogenesis-dependent, which provide necessary nutrient for further growth and metastasis of tumor cells.[4,5]

Angiogenesis is regulated by several endogenous molecules. Vascular endothelial growth factor receptors (VEGFRs) are transmembrane tyrosine kinases consisting of three structurally related isoforms. The binding of VEGFR with its cognate ligand activates several downstream signal cascades, which are responsible for cell proliferation and survival.[2] VEGFR-2 is considered the major mediator, and is a valid target for drug discovery.[6–8] In addition, increasing studies indicate that VEGFR-1 and VEGFR-3 are independently up-regulated in several human malignancies, such as prostate, lung, and colorectal tumors. Higher levels of these receptors are commonly correlated with formation of metastasis.[9–11] These findings highlighted the importance of VEGFR family in tumorigenesis. Platelet-derived growth factor (PDGF) and its cognate receptor mediate an essential signaling for growth of perivascular smooth muscle and pericytes, which are important for neovascularization.[12] Aberrant PDGFRs activation has been documented in clinical samples of tumor such as glioma and prostate cancer, making PDGFRs as druggable therapeutic targets.[13] Upon sustained blockade of VEGF-driven pathway, several other molecules may involve, such as fibroblast growth factor receptor (FGFR), providing a compensatory mechanism to facilitate tumor angiogenesis.[14]

Considering the complicated regulation of tumor angiogenesis, combination therapy and multi-target inhibitors are considered promising strategies to inhibit tumor growth and circumvent drug resistance. On the other hand, the high degree of structural similarities between VEGFR, PDGFR, and FGFR kinases creates possibility to identify inhibitors with synergistic activity. Nintedanib is an authorized inhibitor of VEGFR, PDGFR, and FGFR, with excellent *in vivo* activity in various tumor models.[15] It contains an indolinone scaffold, where by the lactam group forms pivotal hydrogen bonds with the amino acid residues of target proteins.[16,17]

In our previous study, we have disclosed two 6-methoxycarbonyl indolinones (**1** and **2**) as angiokinases inhibitors.[18] Here, our recent work regarding the structural optimizations of these precursors is reported (Fig. 1), which ultimately leads to the discovery of methyl (*Z*)-3-(((4-(2-methyl-5-((4-methylpiperazin-1-yl)methyl)-1*H*-pyrrol-1-yl)phenyl)amino)(phenyl)methylene)-2-oxoindoline-6-carboxylate (**7h**), a more potent multi-kinase inhibitor with excellent antitumor activity.

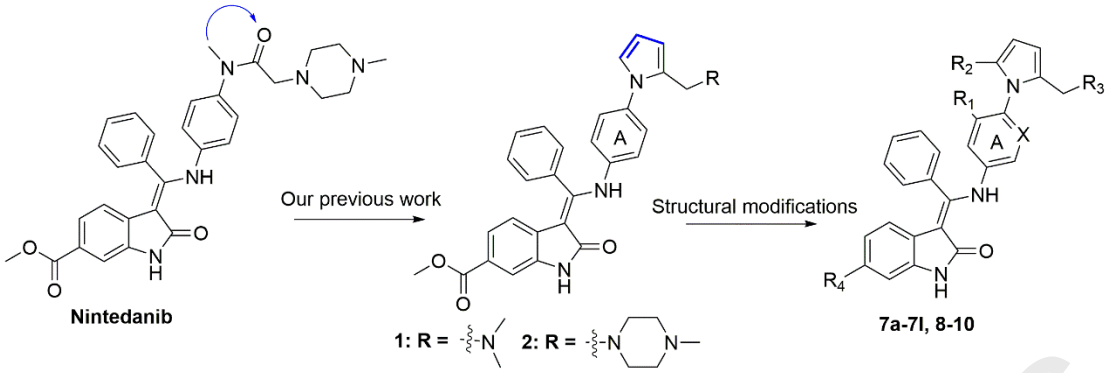

Figure 1. Design strategy of compounds **7a–7l** and **8–10**.

2. Results and discussion

2.1. Chemistry

The synthetic route for preparation of compounds **7a–7l** is outlined in Scheme 1. Briefly, the fluoro benzene or heterocycle **3** underwent a nucleophilic coupling with pyrrole or 2-methyl-1*H*-pyrrole to generate intermediates **4a–4e**, which were converted to intermediates **5a–5l** *via* Mannich reaction followed by hydrogenation reaction as previously reported.[18] Finally, Michael addition reactions were employed by reacting intermediates **5a–5l** with commercially available intermediate methyl (*E*)-3-(methoxy(phenyl)methylene)-2-oxoindoline-6-carboxylate (**6**), to yield the target compounds **7a–7l**.

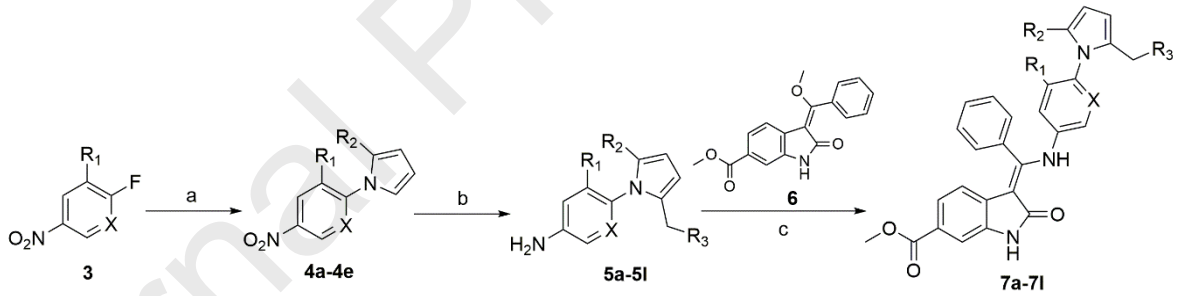

Scheme 1. Reagents and conditions: (a) pyrrole or 2-methyl-1*H*-pyrrole, NaH, DMF, 80 °C, 8–11 h; (b) (i) paraformaldehyde, appropriate amine, HOAc, 35 °C, 6–10 h; (ii) Pd/C, EtOH, 25 °C, 4–6 h; (c) **6**, MeOH, reflux, 4–12 h.

The synthesis of compounds **8–10** is described in Scheme 2. Hydrolysis of ester group of **7h** provided compound **8**, which was reacted with methylamine or dimethylamine to yield compounds **9** and **10**, respectively.

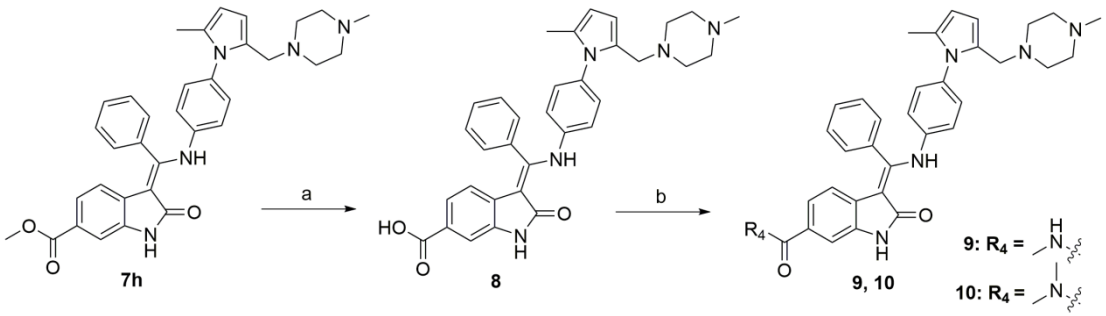

Scheme 2. Reagents and conditions: (a) NaOH, MeOH, reflux, 0.5 h, then HCl; (b) TBTU, HOBT, DIPEA, appropriate amine, DMF, 25 °C, 5 h.

2.2. Biological evaluation

*2.2.1. Modifications of precursors and discovery of compound **7h***

With the intention of discovering more potent angiokinases inhibitors, we undertook a chemistry campaign based on the indolinone precursors. Regarding inhibitors **1** and **2**, we speculated that the dihedral angle between pyrrole and phenyl ring A is crucial for high activity. Thus, from the viewpoint of structure-based drug design, we modified the pyrrole moiety and ring A of them to adjust the dihedral angle, and further to promote their binding with the kinase (Fig. 1). Accordingly, compounds **7a–7l** were prepared and screened for inhibitory activity against VEGFR-2 and PDGFRβ. The parent compounds, **1** and **2**, showed reproducible activity in inhibition of VEGFR-2 and PDGFRβ, with IC_{50} values of 82.3 and 11, 58.3 and 55 nM, respectively.

Initially, we investigated the influence of modified aromatic ring A on activity. Encouraged by the magic methyl group of nintedanib, we first introduced a methyl group and prepared compounds **7a** and **7b**. To our disappointment, as shown in Table 1, both compounds exhibited decreased activity against VEGFR-2 and PDGFRβ than their parent compounds (**7a**, IC_{50} = 492 and 31 nM, respectively; **7b**, IC_{50} = 248 and 206 nM, respectively). Similarly, the replacement of the phenyl ring with heterocyclic bioisostere, pyridine, led to a sharp loss in activity (**7c**, IC_{50} = 472 and 26 nM, respectively; **7d**, IC_{50} = 584 and 114 nM, respectively). Unsurprisingly, combination of the two variations remarkably eroded the enzymatic activity, as shown for **7e** and **7f**. These biological results clearly demonstrated that further modification of aromatic ring A was undesirable. Subsequently, research focus was shifted to the pyrrole moiety, and compounds **7g** and **7h** were readily obtained. Much to our delight, while **7g** showed moderate inhibition of VEGFR-2 and PDGFRβ (IC_{50} = 147.6 and 45.3 nM, respectively), compound **7h** displayed very potent activity, demonstrating IC_{50} values of 6.5 and 9.9 nM, respectively. We speculated that the introduction of the methyl group dramatically tuned the dihedral angle between phenyl ring and pyrrole, which facilitated the formation of ionic interaction between the piperazinyl group with Glu850. Previously, we reported that a dimethylamine or methyl piperazinyl group might represent the optimal amino groups attached to pyrrole.[17,18] To further confirm this speculation, compounds **7i** and **7j** bearing a diethyl amino and morpholinyl group, respectively, were synthesized and evaluated. Both two compounds exhibited promising activity in inhibition of selected kinases, demonstrating IC_{50} values ranging 23.8–227.7 nM, but were less activity as compared to compound **7h**. Furthermore, the replacement of phenyl ring of compound **7h** with pyridine also failed to improve enzymatic inhibitory activity (**7l**, VEGFR-2, IC_{50} = 288 nM; PDGFRβ, IC_{50} = 123 nM).

It was reported that the cleavage of ester was a major metabolic pathway of nintedanib.[15,19] To simulate the metabolic process of **7h**, we prepared its hydrolysis product, **8**. Interestingly, compound **8** also showed excellent activity in inhibition of VEGFR-2 (IC_{50} = 14 nM). The replacement of the ester group with amide fragment

led to compounds **9** and **10**, both of which showed reduced activity.

Table 1. Inhibitory activities of compounds against VEGFR-2 and PDGFRβ.

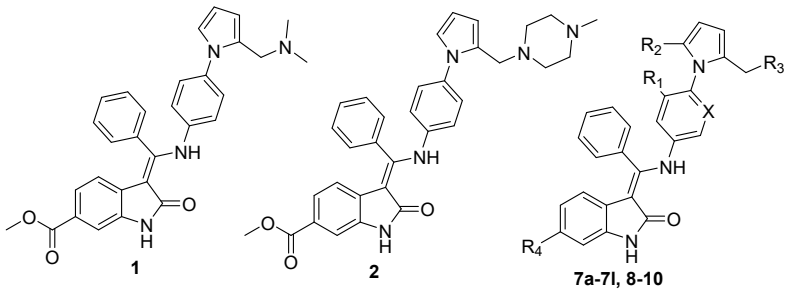

Compound	X	R_1	R_2	R_3	R_4	IC_{50} (nM)[a]	
						VEGFR-2	PDGFRβ
1						82.3 ± 6.3	11 ± 0.6
2						58.3 ± 5.9	55 ± 2.6
7a	C	methyl	H			492 ± 37.8	31 ± 2.2
7b	C	methyl	H			248 ± 35.6	206 ± 11.3
7c	N	H	H			472 ± 22.7	26 ± 3.9
7d	N	H	H			584 ± 27.6	114 ± 5.8
7e	N	methyl	H			>1000	71 ± 3.1
7f	N	methyl	H			>1000	>300
7g	C	H	methyl			147.6 ± 9.7	45.3 ± 6.9
7h	C	H	methyl			6.5 ± 0.9	9.9 ± 0.7
7i	C	H	methyl			100.8 ± 17.6	23.8 ± 3.3
7j	C	H	methyl			227.7 ± 16	37 ± 1.9
7k	N	H	methyl			700 ± 55.6	32 ± 2.7

7l	N	H	methyl			288 ± 30.5	123 ± 15.2
8	C	H	methyl			14 ± 2	NT
9	C	H	methyl			485 ± 37.2	NT
10	C	H	methyl			65 ± 6.7	NT
nintedanib						4.7 ± 0.3	3.8 ± 0.4

NT: not test.

[a] The biological data are generated from at least two independent experiments.

*2.2.2. Kinase inhibition profile of **7h***

Through the structural modification strategy, compound **7h** was identified as a promising inhibitor of angiokinases, although the potency was slightly less active than nintedanib. To further confirm the biological targets of **7h**, we evaluated it in a panel of kinases correlated with tumor growth (Table 2). In addition to VEGFR-2 and PDGFRβ, **7h** displayed strong inhibition of VEGFR-1, VEGFR-3, PDGFRα, and FGFR1 with IC_{50} values ranging 6.3–31 nM, confirming its potent efficacy against angiokinases. It could be noted that **7h** demonstrated moderate activity against SRC (IC_{50} = 178 nM), while showed an excellent inhibition of LYN kinase (IC_{50} = 16 nM). Recent studies have shown that Src-family members played an important role for proliferation of cancer stem cells.[20] Synergistic inhibition of Src-family by **7h** might help for treating cancer. Also, **7h** exhibited excellent inhibitory activity against c-KIT kinase (IC_{50} = 17 nM), which was considered an oncogenic driver in a variety of human cancers such as melanomas.[21] Selected kinases including CDK2, CDK4, CHK, and B-Raf were not significantly inhibited at 1 μM concentration, which indicated that compound **7h** possessed favorable kinase selectivity to a certain degree.

Table 2. Inhibitory activities of compound **7h** against selected kinases.

	IC_{50} (nM)[a]	
Enzyme	7h	Nintedanib
VEGFR-1	31 ± 2.1	23 ± 0.8
VEGFR-2	6.5 ± 0.9	4.7 ± 0.3
VEGFR-3	6.3 ± 0.5	3.0 ± 0.2
PDGFRα	7.0 ± 0.1	1.9 ± 0.3
PDGFRβ	9.9 ± 0.7	3.8 ± 0.4
FGFR-1	23 ± 2.5	99 ± 8.9
SRC	178 ± 15	16 ± 2.1
LYN	16 ± 1.3	55 ± 2.8
c-KIT	17 ± 0.5	NT

CDK2	>1000	>1000
CDK4	>1000	NT
CHK	>1000	>1000
B-Raf	>1000	NT

NT: not test.

[a] The biological data are generated from at least two independent experiments.

*2.2.3. Western blotting analysis of **7h***

Considering that compound **7h** was a potent multi-kinase inhibitor, we analyzed its effects on the phosphorylation of AKT and ERK proteins, which were important downstream signaling effectors of receptor tyrosine kinases. Representative cancer cell lines (HT-29 and HepG2) were treated with **7h** at different concentrations. As shown in Figure 2, **7h** suppressed the phosphorylation of AKT (Ser473) in a dose-dependent manner with a significant inhibition of ERK (Thr202/Tyr204) phosphorylation at 3 μM in both tested cancer cell lines.

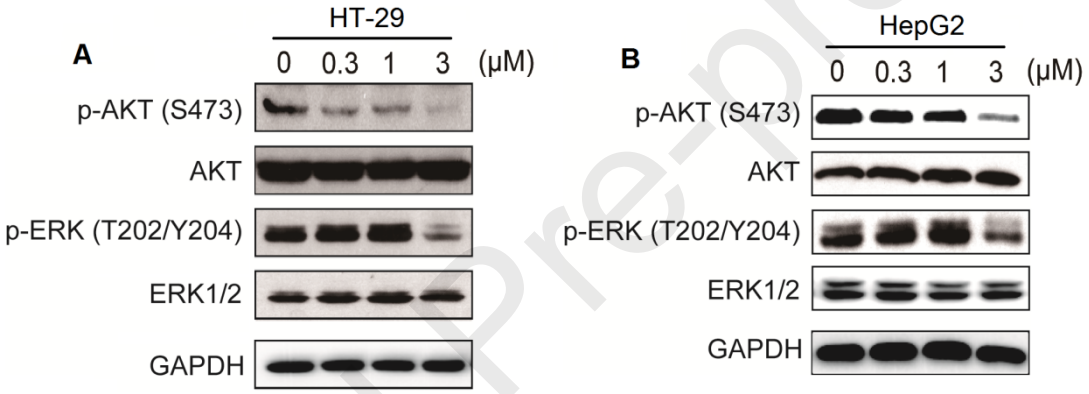

Figure 2. The suppressive effects of **7h** on p-AKT (Ser473) and p-ERK (Thr202/Tyr204) in HT-29 (A) and HepG2 (B) cells.

*2.2.4. Inhibition of colony formation by **7h***

To elucidate the impact of **7h** on proliferation of cancer cells, colony formation assays were performed. HT-29, MKN74, and HepG2 cancer cells were treated with **7h** at indicated concentrations, respectively. As shown in Figure 3, **7h** exhibited excellent activity in inhibition of colony formations in a dose-dependent manner, with remarkable activity at 1 μM concentration for all tested cancer cells. With respect to MKN74 cancer cells, treatment with 1 μM **7h** almost completely suppressed the colony formation, and was more active than nintedanib.

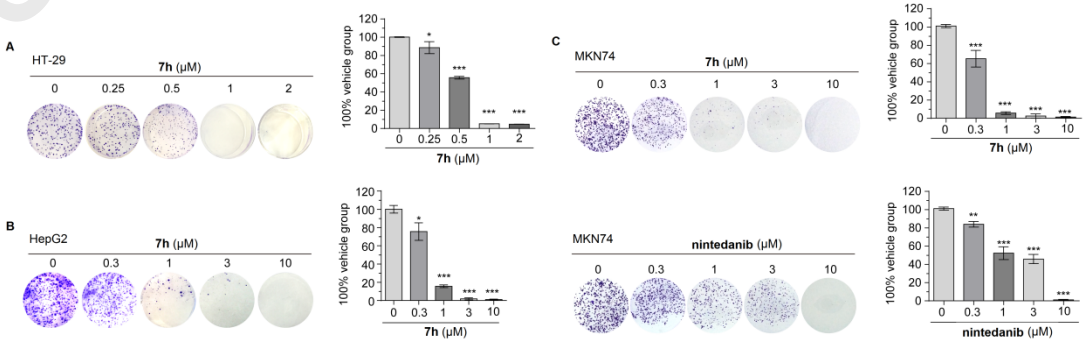

Figure 3. Colony formation of HT-29 (A), HepG2 (B), and MKN74 cells (C) treated with **7h** and nintedanib. Relative colony formation rate is shown as mean ± SEM. *P < 0.05, **P < 0.01, and ***P < 0.001 versus vehicle group; P-values were calculated using an unpaired two-tailed Student's *t*-test.

*2.2.5. Induction of cell apoptosis by **7h***

A biparametric cytofluorimetric analysis was conducted to evaluate the effects of **7h** on cancer cells apoptosis. As shown in Figure 4, **7h** triggered severe apoptosis of HT-29, MKN74, and HepG2 cells in a dose-dependent manner. Human umbilical vein endothelial cells (HUVECs) were used to evaluate the effects of **7h** on endothelial cells, the proliferation of which was considered a critical process of angiogenesis. Significantly, the apoptotic rate of HUVECs was increased from 7.11% (control) to 64.69% in the 3 μM group. In contrast, no significant induction of apoptosis was observed in normal cells HEK293T (Fig. S1).

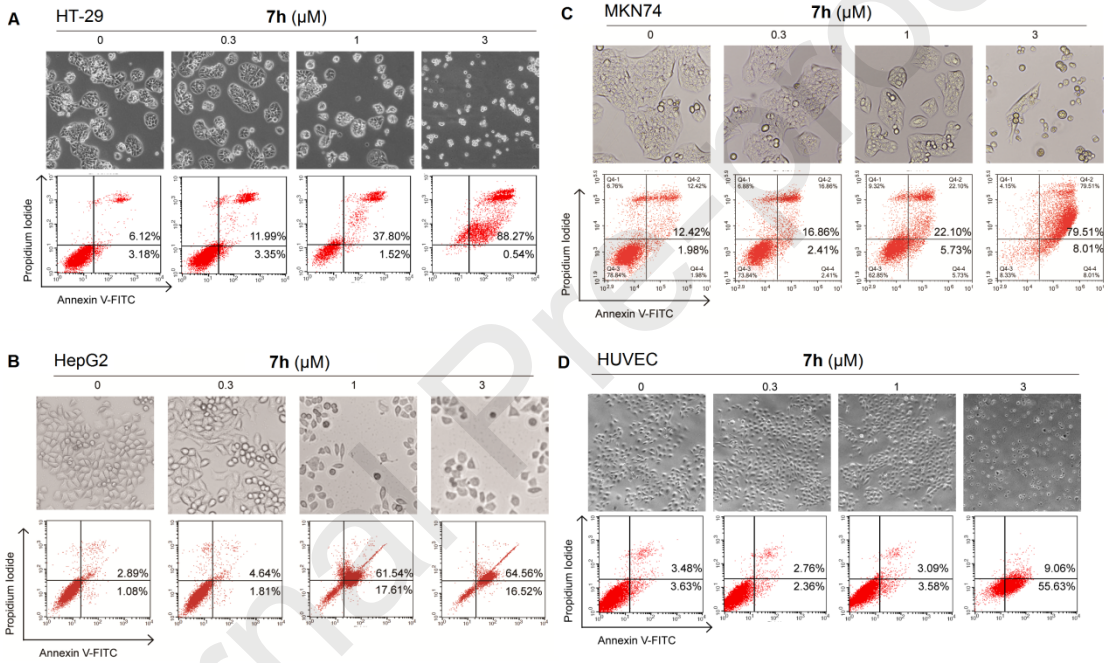

Figure 4. Effects of **7h** on cell apoptosis in HT-29 (A), HepG2 (B), MKN74 (C), and HUVEC (D) cells.

*2.2.6. In vitro metabolic stability of **7h***

Compound **7h** was incubated with human and mouse liver microsomes, respectively, to evaluate the metabolic stability *in vitro*. The results in Table 3 revealed that **7h** (Cl_{int} = 81.97 mL/min/kg) suffered slightly higher clearance upon incubation with human microsome than that of nintedanib (Cl_{int} = 63.5 mL/min/kg), and thus possessed a relatively shorter $T_{1/2}$ (21.21 min *vs* 27.38 min). Detailed pharmacokinetic profile of **7h** should be further assessed in *in vivo* experiments.

Table 3. Liver microsomal stability of compound **7h**.

Compound	Human		Mouse	
	$T_{1/2}$ (min)	Cl_{int} (mL/min/kg)	$T_{1/2}$ (min)	Cl_{int} (mL/min/kg)
7h	21.21	81.97	12.53	435.65

Nintedanib	27.38	63.5	-	-

*2.2.7. In vivo antitumor activity of **7h***

Considering high levels of biological activity and moderate metabolic stability, compound **7h** was evaluated for *in vivo* activity in a HT-29 human colon cancer xenograft model. Nude mice bearing established HT-29 tumor xenografts were dosed orally for 18 days. Compound **7h** (100 mg/kg, qd) displayed mild inhibition of tumor growth, with tumor growth inhibition (TGI) value of 13.39% while that of nintedanib (100 mg/kg, qd) was 44.27% (Figure 5). The tested compound was well-tolerated, no significant loss of body weight was observed during treatment.

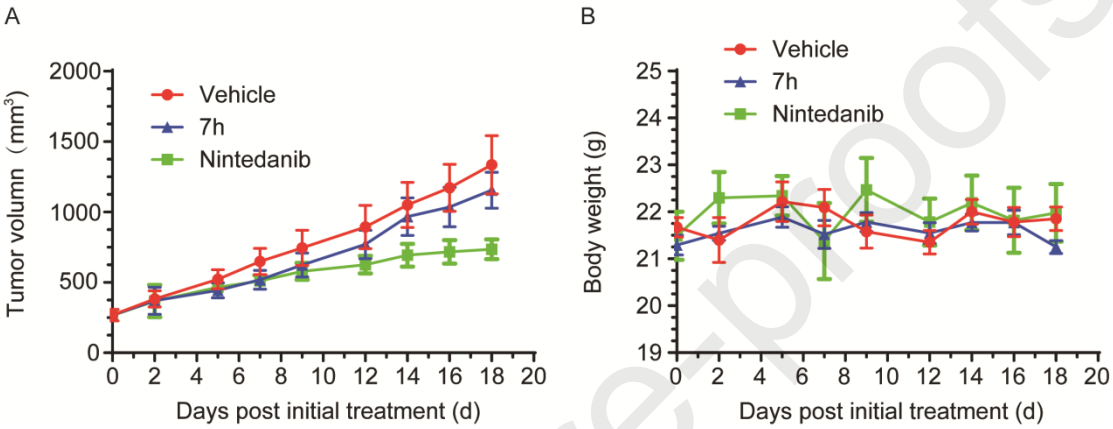

Figure 5. *In vivo* effect of compound **7h** on tumor volume (A) and body weight (B) in xenograft model of HT-29. Mice were orally dosed once daily for 18 days at 100mg/kg. Results are expressed as the mean ± SD. (n = 6 per group).

2.3. Molecular docking study

Docking study of compound **7h** at the ATP-binding site of VEGFR-2 was performed to explore its probable binding mode. The crystal structure of VEGFR-2 kinase domain was obtained from the Protein Data Bank (PDB code: 3C7Q). As shown in Figure 6A, **7h** matched well with this binding site, accounting for its high *in vitro* activity in inhibition of VEGFR-2. Three hydrogen bonds were formed between the 6-methoxycarbonyl indolinone moiety of **7h** with Glu917, Cys919, and Lys868 in the hinge region. Particularly, the piperazinyl group interacted with Glu850 *via* an ionic interaction as well as a carbon hydrogen bond, which further improved inhibitor binding. Figure 6B showed the high-degree overlay of **7h** and nintedanib at this binding site.

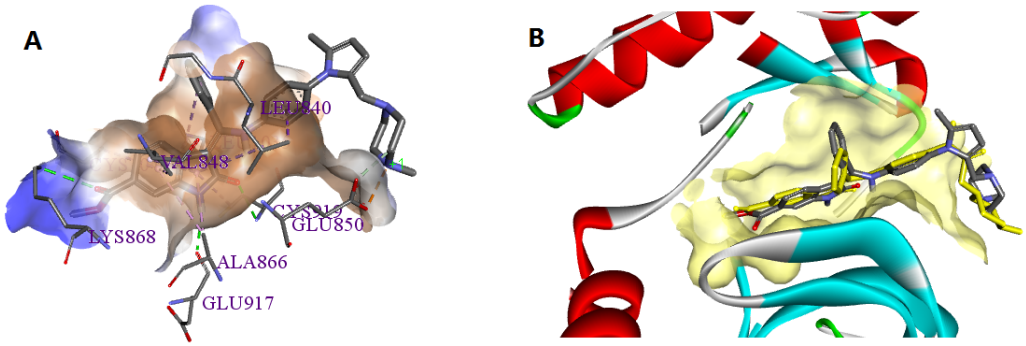

Figure 6. (A) Probable interactions between compound **7h** and VEGFR-2. Dashed lines indicated the contacts between the inhibitor and selected residues. (B) Binding model overlap of compound **7h** (grey) and nintedanib (yellow) at the binding site.

3. Conclusions

In summary, structural modifications of compound **2**, an angiokinase inhibitor reported previously were performed in this study, which generated a potent multi-kinase inhibitor, **7h**, for the treatment of tumor. Compound **7h** exhibited excellent potency against angiokinases, with IC_{50} values ranging 6.3–31 nM. Also, it displayed potent activity against other kinases correlated with tumor growth, such as LYN and c-KIT kinases. In cells, **7h** effectively attenuated the phosphorylation of AKT and ERK proteins. Significant anti-proliferative activity was also exhibited by **7h**, which potently inhibited colony formation of HT-29, HepG2, and MKN74 cancer cells, and induced cell apoptosis. Molecular docking analysis demonstrated that **7h** matched well with the active site of VEGFR-2, and the ionic interaction between piperazinyl group and Glu850 was crucial for high kinase affinity, which contributed to excellent *in vitro* activity of **7h**. Nonetheless, in our initial *in vivo* study with **7h** in a HT-29 xenograft model, effects on growth of tumor were only mild. The results might be ascribed to its relatively high hepatic clearance as exhibited in an *in vitro* assay.

The structure-activity relationships of the newly synthesized compounds were explored, providing valuable information for the future work. For example, modifications of aromatic ring A were unsuitable, but further investigations on 6-position of indolinone moiety were deserved. In future studies, structural modifications of **7h** are warranted to improve its pharmacokinetic property, and thus, excellent *in vivo* antitumor activity can be expected.

4. Experimental section

4.1. Chemistry

Reagents and solvents were obtained from commercial sources and used without further purification. All the reactions were monitored by TLC using silica gel GF/UV 254. Flash chromatography was performed using silica gel (300–400 mesh). The purity of the synthesized compounds was measured by high performance liquid chromatography (HPLC, Agilent, USA), and was confirmed to be higher than 95%. Melting points were determined on a Büchi Melting Point B-540 apparatus (Büchi Labortechnik, Flawil, Switzerland). The ^{1}H and ^{13}C NMR spectra were recorded on Bruker AV-400 spectrometer, with TMS as an internal standard. The low resolution of ESI-MS was recorded on an Agilent 1100 LC-MS spectrometer, and high resolution mass spectrometry was performed on an Agilent Accurate-Mass Q-TOF 6530 in ESI mode.

*4.1.1. General procedure for preparation of compounds **4a–4e***

To a solution of pyrrole or 2-methyl-1*H*-pyrrole (0.15 mol) in DMF (100 mL), NaH (0.195 mol, 60%) was added in portions, then appropriate intermediate **3** was added dropwise. The mixture was stirred at 80 °C for 8–11 h, and was monitored by TLC. The mixture was poured into ice water, and stirred for 15 min. The precipitate was filtered off to give a crude product, which was purified by column

chromatography to give the desired compound.

*4.1.1.1. 1-(2-Methyl-4-nitrophenyl)-1H-pyrrole (**4a**).* Yellow solid. Yield: 27%. ^{1}H NMR (600 MHz, DMSO-d_6) δ 8.30 (s, 1H), 8.14 (s, 1H), 7.52 (s, 1H), 7.09 (s, 2H), 6.31 (s, 2H), 2.37 (s, 3H). ESI-MS m/z: 203.1 $[M+H]^+$.

*4.1.1.2. 5-Nitro-2-(1H-pyrrol-1-yl)pyridine (**4b**).* Yellow solid. Yield: 41%. ^{1}H NMR (600 MHz, DMSO-d_6) δ 9.25 (s, 1H), 8.68 (dd, J = 9.1, 2.7 Hz, 1H), 7.96 (d, J = 9.1 Hz, 1H), 7.81 (s, 2H), 6.42 (m, 2H). ESI-MS m/z: 190.1 $[M+H]^+$.

*4.1.1.3. 3-Methyl-5-nitro-2-(1H-pyrrol-1-yl)pyridine (**4c**).* Yellow solid. Yield: 56%. ^{1}H NMR (600 MHz, DMSO-d_6) δ 9.15 (s, 1H), 8.70 (s, 1H), 7.43 (s, 2H), 6.35 (s, 2H), 2.50 (s, 3H). ESI-MS m/z: 204.1 $[M+H]^+$.

*4.1.1.4. 2-Methyl-1-(4-nitrophenyl)-1H-pyrrole (**4d**).* Yellow solid. Yield: 36%. ^{1}H NMR (600 MHz, DMSO-d_6) δ 8.34 (m, 1H), 8.33 (m, 1H), 7.70 (m, 1H), 7.69 (m, 1H), 7.02 (s, 1H), 6.19 (s, 1H), 6.08 (s, 1H), 2.27 (s, 3H). ESI-MS m/z: 203.1 $[M+H]^+$.

*4.1.1.5. 2-(2-Methyl-1H-pyrrol-1-yl)-5-nitropyridine (**4e**).* Yellow solid. Yield: 53%. ^{1}H NMR (600 MHz, DMSO-d_6) δ 9.28 (s, 1H), 8.66 (s, 1H), 7.82 (s, 1H), 7.41 (s, 1H), 6.23 (s, 1H), 6.11 (s, 1H), 2.49 (s, 3H). ESI-MS m/z: 204.1 $[M+H]^+$.

*4.1.2. General procedure for preparation of compounds **5a–5l***

To a mixture of paraformaldehyde (15 mmol) and appropriate secondary amine (15 mmol) in acetic acid (5 mL) was added intermediate **4a–4e** (10 mmol). The solution was stirred at 35 °C for 6–10 h, and was monitored by TLC. After that time, the acetic acid was concentrated. The residue was diluted with ethanol (15 mL), and Pd/C (10%) was added. The reaction mixture was hydrogenated for 4–6 h. When TLC showed the completion of the reaction, the catalyst was filtered off, then the solvent was evaporated. The residue was purified by column chromatography to afford the desired intermediate.

*4.1.2.1. 4-(2-((Dimethylamino)methyl)-1H-pyrrol-1-yl)-3-methylaniline (**5a**).* Yellow solid. Yield: 16%. ESI-MS m/z: 230.1 $[M+H]^+$.

*4.1.2.2. 3-Methyl-4-(2-((4-methylpiperazin-1-yl)methyl)-1H-pyrrol-1-yl)aniline (**5b**).* Yellow solid. Yield: 22%. ESI-MS m/z: 285.2 $[M+H]^+$.

*4.1.2.3. 6-(2-((Dimethylamino)methyl)-1H-pyrrol-1-yl)pyridin-3-amine (**5c**).* Yellow solid. Yield: 37%. ESI-MS m/z: 217.1 $[M+H]^+$.

*4.1.2.4. 6-(2-((4-Methylpiperazin-1-yl)methyl)-1H-pyrrol-1-yl)pyridin-3-amine (**5d**).* Yellow solid. Yield: 26%. ESI-MS m/z: 272.2 $[M+H]^+$.

*4.1.2.5. 6-(2-((Dimethylamino)methyl)-1H-pyrrol-1-yl)-5-methylpyridin-3-amine (**5e**).* Yellow solid. Yield: 19%. ESI-MS m/z: 231.2 $[M+H]^+$.

4.1.2.6.
*5-Methyl-6-(2-((4-methylpiperazin-1-yl)methyl)-1H-pyrrol-1-yl)pyridin-3-amine (**5f**).* Yellow solid. Yield: 23%. ESI-MS m/z: 286.2 $[M+H]^+$.

*4.1.2.7. 4-(2-((Dimethylamino)methyl)-5-methyl-1H-pyrrol-1-yl)aniline (**5g**).* Yellow solid. Yield: 39%. ^{1}H NMR (400 MHz, DMSO-d_6) δ 6.90 (d, J = 8.3 Hz, 2H), 6.64 (d, J = 8.3 Hz, 2H), 6.35 (d, J = 2.5 Hz, 1H), 5.92 (d, J = 2.6 Hz,1H), 5.42 (s, 2H), 3.79 (s, 2H), 2.37 (s, 6H), 1.93 (s, 3H). ESI-MS m/z: 230.2 $[M+H]^+$.

*4.1.2.8. 4-(2-Methyl-5-((4-methylpiperazin-1-yl)methyl)-1H-pyrrol-1-yl)aniline (**5h**).*

Yellow solid. Yield: 42%. ^{1}H NMR (600 MHz, DMSO-d_6) δ 8.37 (d, J = 8.8 Hz, 1H), 8.24 (d, J = 8.7 Hz, 1H), 7.64 (d, J = 8.8 Hz, 1H), 7.56 (d, J = 8.7 Hz, 1H), 6.00 (dd, J = 14.2, 3.3 Hz, 1H), 5.91 (dd, J = 13.8, 3.1 Hz, 1H), 3.18 (d, J = 6.4 Hz, 2H), 2.43–1.92 (m, 14H). ESI-MS m/z: 285.2 $[M+H]^+$.

*4.1.2.9. 4-(2-((Diethylamino)methyl)-5-methyl-1H-pyrrol-1-yl)aniline (**5i**).* Yellow solid. Yield: 21%. ESI-MS m/z: 258.2 $[M+H]^+$.

*4.1.2.10. 4-(2-Methyl-5-(morpholinomethyl)-1H-pyrrol-1-yl)aniline (**5j**).* Yellow solid. Yield: 17%. ESI-MS m/z: 272.2 $[M+H]^+$.

*4.1.2.11. 6-(2-((Dimethylamino)methyl)-5-methyl-1H-pyrrol-1-yl)pyridin-3-amine (**5k**).* Yellow solid. Yield: 30%. ESI-MS m/z: 231.2 $[M+H]^+$.

*4.1.2.12. 6-(2-Methyl-5-((4-methylpiperazin-1-yl)methyl)-1H-pyrrol-1-yl)pyridin-3-amine (**5l**).* Yellow solid. Yield: 24%. ESI-MS m/z: 286.2 $[M+H]^+$.

*4.1.3. General procedure for preparation of compounds **7a–7l***

At room temperature, to a solution of intermediate (**5a–5l**, 0.2 mmol) in methanol (7 mL) was added intermediate methyl (*E*)-3-(methoxy(phenyl)methylene)-2-oxoindoline-6-carboxylate (0.2 mmol). The mixture was stirred under reflux for 4–12 h and was monitored by TLC. Upon completion of the reaction, the solution was cooled, the precipitate was filtered off to give a crude product, which was recrystallized from methanol to afford the target compound.

*4.1.3.1. Methyl (Z)-3-(((4-(2-((dimethylamino)methyl)-1H-pyrrol-1-yl)-3-methylphenyl)amino)(phenyl)methylene)-2-oxoindoline-6-carboxylate (**7a**).* Yellow solid. Yield: 72%. Mp: 219.7–221.2 °C. ^{1}H NMR (600 MHz, DMSO-d_6) δ 12.26 (s, 1H), 11.01 (s, 1H), 7.62 (d, J = 7.0 Hz, 1H), 7.59 (t, J = 6.9 Hz, 2H), 7.53 (d, J = 6.4 Hz, 2H), 7.44 (s, 1H), 7.21 (d, J = 7.9 Hz, 1H), 6.99 (d, J = 8.3 Hz, 1H), 6.91 (s, 1H), 6.68–6.62 (m, 2H), 6.08 (s, 1H), 6.04 (s, 1H), 5.87 (d, J = 8.1 Hz, 1H), 3.78 (s, 3H), 2.91 (s, 2H), 1.89 (s, 6H), 1.79 (s, 3H). HRMS (ESI) for $C_{31}H_{30}N_4O_3$ $[M + H]^+$, calcd: 507.2391, found: 507.2397.

*4.1.3.2. Methyl (Z)-3-(((3-methyl-4-(2-((4-methylpiperazin-1-yl)methyl)-1H-pyrrol-1-yl)phenyl)amino)(phenyl)methylene)-2-oxoindoline-6-carboxylate (**7b**).* Yellow solid. Yield: 68%. Mp: 262.2–264.7 °C. ^{1}H NMR (600 MHz, DMSO-d_6) δ 12.25 (s, 1H), 10.99 (s, 1H), 7.64–7.60 (m, 1H), 7.58 (t, J = 7.3 Hz, 2H), 7.53 (s, 2H), 7.43 (d, J = 1.4 Hz, 1H), 7.21 (dd, J = 8.2, 1.5 Hz, 1H), 7.01 (d, J = 8.4 Hz, 1H), 6.92 (d, J = 2.3 Hz, 1H), 6.65 (dt, J = 6.4, 3.0 Hz, 2H), 6.06 (t, J = 3.1 Hz, 1H), 6.02 (dd, J = 3.2, 1.6 Hz, 1H), 5.86 (d, J = 8.2 Hz, 1H), 3.78 (s, 3H), 2.97 (s, 2H), 2.10 (s, 3H), 2.04 (br, 8H), 1.81 (s, 3H). ^{13}C NMR (151 MHz, DMSO-d_6) δ 170.60, 166.77, 158.77, 138.04, 136.96, 136.65, 135.69, 132.46, 130.86, 129.85, 129.32, 128.97, 128.83, 128.78, 125.09, 124.47, 123.03, 121.90, 120.92, 117.71, 109.88, 109.52, 107.76, 98.02, 54.18, 52.84, 52.20, 50.90, 44.51, 17.41. HRMS (ESI) for $C_{34}H_{35}N_5O_3$ $[M + H]^+$, calcd: 562.2813, found: 562.2818.

4.1.3.3. Methyl (Z)-3-((((6-(2-((dimethylamino)methyl)-1H-pyrrol-1-yl)pyridin-3-yl)amino)(phenyl)me

*thylene)-2-oxoindoline-6-carboxylate (**7c**).* Yellow solid. Yield: 53%. Mp: 216.7–219.3 °C. ^{1}H NMR (400 MHz, DMSO-d_6) δ 12.19 (s, 1H), 11.08 (s, 1H), 8.18 (s, 1H), 7.67–7.50 (m, 6H), 7.44 (t, J = 7.2 Hz, 1H), 7.38 (dd, J = 8.8, 2.5 Hz, 2H), 7.22 (dd, J = 8.2, 1.4 Hz, 1H), 6.36 (s, 1H), 6.22 (s, 1H), 5.89 (d, J = 8.2 Hz, 1H), 3.93 (s, 2H), 3.78 (s, 3H), 2.42 (s, 6H). ^{13}C NMR (101 MHz, DMSO-d_6) δ 170.68, 166.82, 158.60, 148.32, 143.58, 137.06, 134.39, 133.36, 132.07, 131.23, 131.15, 130.11, 129.18, 129.13, 124.94, 122.97, 122.07, 118.01, 116.11, 116.08, 110.69, 110.07, 98.96, 54.51, 52.31, 43.38. HRMS (ESI) for $C_{29}H_{27}N_5O_3$ $[M + H]^+$, calcd: 494.2187, found: 494.2183.

*4.1.3.4. Methyl (Z)-3-(((6-(2-((4-methylpiperazin-1-yl)methyl)-1H-pyrrol-1-yl)pyridin-3-yl)amino)(phenyl)methylene)-2-oxoindoline-6-carboxylate (**7d**).* Yellow solid. Yield: 71%. Mp: 257.3–261.3 °C. ^{1}H NMR (400 MHz, DMSO-d_6) δ 12.13 (s, 1H), 11.03 (s, 1H), 8.05 (d, J = 2.3 Hz, 1H), 7.63–7.51 (m, 6H), 7.48–7.38 (m, 2H), 7.22 (dd, J = 8.2, 1.5 Hz, 1H), 7.17 (s, 1H), 6.19–6.06 (m, 2H), 5.87 (d, J = 8.2 Hz, 1H), 3.78 (s, 3H), 3.53 (s, 3H), 3.17 (s, 2H), 2.31 (br, 8H). ^{13}C NMR (101 MHz, DMSO-d_6) δ 170.66, 166.83, 158.80, 148.92, 143.76, 136.99, 134.07, 133.28, 132.17, 131.07, 130.02, 129.25, 129.14, 124.84, 122.29, 122.23, 122.05, 117.96, 117.13, 117.11, 110.00, 108.99, 98.73, 54.37, 53.72, 52.31, 51.16, 49.06. HRMS (ESI) for $C_{32}H_{32}N_6O_3$ $[M + H]^+$, calcd: 549.2609, found: 549.2616.

*4.1.3.5. Methyl (Z)-3-(((6-(2-((dimethylamino)methyl)-1H-pyrrol-1-yl)-5-methylpyridin-3-yl)amino)(phenyl)methylene)-2-oxoindoline-6-carboxylate (**7e**).* Yellow solid. Yield: 71%. Mp: 132.6.2–135.1 °C. ^{1}H NMR (400 MHz, DMSO-d_6) δ 12.15 (s, 1H), 11.04 (s, 1H), 7.82 (s, 1H), 7.55 (m, 7H), 7.22 (d, J = 7.6 Hz, 1H), 6.87 (s, 1H), 6.11 (s, 2H), 5.90 (d, J = 8.1 Hz, 1H), 3.78 (s, 3H), 3.27 (s, 2H), 1.95 (br, 9H). ^{13}C NMR (101 MHz, DMSO-d_6) δ 170.68, 166.80, 158.53, 150.29, 147.82, 141.02, 137.08, 134.89, 134.78, 132.17, 131.09, 130.11, 130.03, 129.17, 129.10, 124.98, 122.69, 122.08, 118.06, 110.03, 108.15, 99.00, 94.32, 54.23, 52.31, 44.40, 17.53. HRMS (ESI) for $C_{30}H_{29}N_5O_3$ $[M + H]^+$, calcd: 508.2343, found: 508.2350.

*4.1.3.6. Methyl (Z)-3-(((5-methyl-6-(2-((4-methylpiperazin-1-yl)methyl)-1H-pyrrol-1-yl)pyridin-3-yl)amino)(phenyl)methylene)-2-oxoindoline-6-carboxylate (**7f**).* Yellow solid. Yield: 46%. Mp: 134.3–137.0 °C. ^{1}H NMR (400 MHz, DMSO-d_6) δ 12.15 (s, 1H), 11.08 (s, 1H), 7.81 (s, 1H), 7.62 (m, 3H), 7.55 (m, 2H), 7.45 (s, 1H), 7.41 (s, 1H), 7.22 (d, J = 8.2 Hz, 1H), 6.83 (s, 1H), 6.06 (s, 2H), 5.87 (d, J = 8.2 Hz, 1H), 3.78 (s, 3H), 3.42 (s, 3H), 3.33 (s, 2H), 2.33 (s, 4H), 2.14 (s, 4H), 1.93 (s, 3H). ^{13}C NMR (101 MHz, DMSO-d_6) δ 170.65, 166.81, 158.54, 148.14, 140.90, 137.08, 134.90, 134.44, 132.23, 131.11, 130.62, 130.45, 130.04, 129.18, 129.04, 124.96, 122.47, 122.07, 118.03, 110.05, 109.88, 107.89, 98.99, 56.48, 54.00, 52.90, 52.31, 19.02. HRMS (ESI) for $C_{33}H_{34}N_6O_3$ $[M + H]^+$, calcd: 563.2765, found: 563.2761.

*4.1.3.7. Methyl (Z)-3-(((4-(2-((dimethylamino)methyl)-5-methyl-1H-pyrrol-1-yl)phenyl)amino)(phenyl)methylene)-2-oxoindoline-6-carboxylate (**7g**).* Yellow solid. Yield: 58%. Mp: 216.7–

219.3 °C. ^{1}H NMR (400 MHz, DMSO-d_6) δ 12.25 (s, 1H), 10.99 (s, 1H), 7.58 (m, 3H), 7.54–7.51 (m, 2H), 7.43 (d, *J* = 1.0 Hz, 1H), 7.21 (dd, *J* = 8.3, 1.3 Hz, 1H), 7.12 (d, *J* = 8.6 Hz, 2H), 6.97 (d, *J* = 8.6 Hz, 2H), 5.90 (dd, *J* = 13.7, 4.7 Hz, 2H), 5.82 (d, *J* = 2.6 Hz, 1H), 3.78 (s, 3H), 2.95 (s, 2H), 1.92 (br, 9H). HRMS (ESI) for $C_{31}H_{30}N_4O_3$ $[M + H]^+$, calcd: 507.2391, found: 507.2396.

*4.1.3.8. Methyl (Z)-3-(((4-(2-methyl-5-((4-methylpiperazin-1-yl)methyl)-1H-pyrrol-1-yl)phenyl)amino)(phenyl)methylene)-2-oxoindoline-6-carboxylate (**7h**).* Yellow solid. Yield: 73%. Mp: 200.2–203.2 °C. ^{1}H NMR (600 MHz, DMSO-d_6) δ 12.25 (s, 1H), 10.98 (s, 1H), 7.60 (dt, *J* = 2.7, 2.0 Hz,1H), 7.56 (m, 2H), 7.52 (dd, *J* = 8.0, 1.3 Hz, 2H), 7.43 (d, *J* = 1.4 Hz, 1H), 7.21 (dd, *J* = 8.2, 1.6 Hz, 1H), 7.13 (d, *J* = 8.7 Hz, 2H), 6.95 (d, *J* = 8.7 Hz, 2H), 5.88 (m, 2H), 5.80–5.78 (m, 1H), 3.78 (s, 3H), 2.94 (s, 2H), 2.18–2.11 (br, 11H), 1.91 (s, 3H). ^{13}C NMR (151 MHz, DMSO-d_6) δ 170.61, 166.78, 158.94, 137.62, 136.65, 135.13, 132.40, 130.83, 129.76, 129.37, 129.28, 129.13, 129.06, 128.94, 124.43, 123.90, 121.88, 117.70, 109.85, 108.83, 106.31, 97.98, 55.13, 53.73, 52.19, 52.17, 46.08, 13.07. HRMS (ESI) for $C_{34}H_{35}N_5O_3$ $[M + H]^+$, calcd: 562.2813, found: 562.2817.

*4.1.3.9. Methyl (Z)-3-(((4-(2-((diethylamino)methyl)-5-methyl-1H-pyrrol-1-yl)phenyl)amino)(phenyl)methylene)-2-oxoindoline-6-carboxylate (**7i**).* Yellow solid. Yield: 63%. Mp: 232.0–235.3 °C. ^{1}H NMR (600 MHz, DMSO-d_6) δ 12.25 (s, 1H), 10.99 (s, 1H), 7.62–7.59 (m, 1H), 7.57 (m, 2H), 7.52 (d, *J* = 7.5 Hz, 2H), 7.44 (s, 1H), 7.21 (d, *J* = 8.2 Hz, 1H), 7.09 (d, *J* = 8.5 Hz, 2H), 6.95 (d, *J* = 8.5 Hz, 2H), 5.89 (d, *J* = 3.1 Hz, 1H), 5.86 (d, *J* = 8.2 Hz, 1H), 5.79 (d, *J* = 2.9 Hz, 1H), 3.78 (s, 3H), 3.09 (s, 2H), 2.20 (q, *J* = 7.0 Hz, 4H), 1.88 (s, 3H), 0.65 (t, *J* = 7.0 Hz, 6H). ^{13}C NMR (151 MHz, DMSO-d_6) δ 170.61, 166.79, 158.92, 137.61, 136.64, 135.37, 132.34, 130.82, 130.14, 129.82, 129.36, 129.18, 128.98, 128.87, 124.42, 123.86, 121.87, 117.69, 109.86, 108.83, 106.22, 98.02, 52.19, 48.80, 45.80, 13.05, 11.77. HRMS (ESI) for $C_{33}H_{34}N_4O_3$ $[M + H]^+$, calcd: 535.2704, found: 535.2711.

*4.1.3.10. Methyl (Z)-3-(((4-(2-methyl-5-(morpholinomethyl)-1H-pyrrol-1-yl)phenyl)amino)(phenyl)methylene)-2-oxoindoline-6-carboxylate (**7j**).* Yellow solid. Yield: 70%. Mp: 241.0–242.7 °C. ^{1}H NMR (400 MHz, DMSO-d_6) δ 12.24 (s, 1H), 10.99 (s, 1H), 7.61–7.54 (m, 3H), 7.52 (d, *J* = 6.9 Hz, 2H), 7.43 (d, *J* = 1.1 Hz, 1H), 7.21 (dd, *J* = 8.2, 1.3 Hz, 1H), 7.15 (d, *J* = 8.6 Hz, 2H), 6.96 (d, *J* = 8.6 Hz, 2H), 5.89 (m, 2H), 5.80 (d, *J* = 2.9 Hz, 1H), 3.78 (s, 3H), 3.38 (br, 4H), 2.97 (s, 2H), 2.06 (br, 4H), 1.91 (s, 3H). HRMS (ESI) for $C_{33}H_{32}N_4O_4$ $[M + H]^+$, calcd: 549.2496, found: 549.2500.

*4.1.3.11. Methyl (Z)-3-(((6-(2-((dimethylamino)methyl)-5-methyl-1H-pyrrol-1-yl)pyridin-3-yl)amino)(phenyl)methylene)-2-oxoindoline-6-carboxylate (**7k**).* Yellow solid. Yield: 63%. Mp: 194.7–197.0 °C. ^{1}H NMR (400 MHz, DMSO-d_6) δ 12.16 (s, 1H), 11.05 (s, 1H), 8.17 (d, *J* = 2.3 Hz, 1H), 7.63–7.53 (m, 5H), 7.47–7.42 (m, 2H), 7.38 (d, *J* = 8.6 Hz, 1H), 7.23 (dd, *J* = 8.2, 1.3 Hz, 1H), 6.16 (s, 1H), 5.93 (m, 2H), 3.78 (s, 3H), 3.54 (s, 2H), 2.21 (s, 6H), 2.04 (s, 3H). ^{13}C NMR (101 MHz, DMSO-d_6) δ 170.67, 166.81, 158.49,

144.28, 137.14, 134.61, 133.57, 132.08, 131.14, 130.58, 130.56, 130.04, 129.27, 129.22, 129.16, 125.04, 122.08, 121.66, 118.11, 110.06, 108.65, 108.07, 99.15, 56.49, 52.32, 43.39, 13.45. HRMS (ESI) for $C_{30}H_{29}N_5O_3$ $[M + H]^+$, calcd: 508.2343, found: 508.2341.

*4.1.3.12. Methyl (Z)-3-(((6-(2-methyl-5-((4-methylpiperazin-1-yl)methyl)-1H-pyrrol-1-yl)pyridin-3-yl)amino)(phenyl)methylene)-2-oxoindoline-6-carboxylate (**7l**).* Yellow solid. Yield: 57%. Mp: 217.5–220.1 °C. ^{1}H NMR (400 MHz, DMSO-d_6) δ 12.15 (s, 1H), 11.05 (s, 1H), 8.15 (d, J = 2.3 Hz, 1H), 7.64–7.52 (m, 5H), 7.45 (s, 1H), 7.41–7.30 (m, 2H), 7.23 (d, J = 8.2, 1H), 5.91 (d, J = 8.3 Hz, 2H), 5.81 (d, J = 2.5 Hz, 1H), 3.78 (s, 3H), 3.20 (s, 2H), 2.49–2.03 (br, 11H), 1.97 (s, 3H). ^{13}C NMR (101 MHz, DMSO-d_6) δ 170.67, 166.82, 158.66, 148.04, 144.04, 137.08, 134.40, 133.17, 132.15, 131.08, 129.97, 129.73, 129.18, 128.77, 124.95, 122.13, 122.06, 118.04, 110.03, 109.79, 106.95, 99.99, 98.99, 54.33, 53.50, 52.31, 50.89, 44.81, 13.18. HRMS (ESI) for $C_{33}H_{34}N_6O_3$ $[M + H]^+$, calcd: 563.2765, found: 563.2768.

*4.1.4. (Z)-3-(((4-(2-methyl-5-((4-methylpiperazin-1-yl)methyl)-1H-pyrrol-1-yl)phenyl)amino)(phenyl)methylene)-2-oxoindoline-6-carboxylic acid (**8**).*

To a solution of compound **7h** (0.3 g, 0.53 mmol) in methanol (10 mL) was added 1N NaOH solution (10 mL). The mixture was reflux for 0.5 h until TLC showed the completion of the reaction. The methanol was evaporated, the solution was acidized with 1N HCl solution to pH 6–7. The precipitate was filtered off to give a crude product, which was washed with methanol to give compound **8** (0.15 g, 51.7%) as a yellow solid. Mp: 279.1–283.2 °C. ESI-MS m/z: 548.3 $[M+H]^+$. ^{1}H NMR (400 MHz, DMSO-d_6) δ 12.23 (s, 1H), 10.96 (s, 1H), 7.63–7.57 (m, 3H), 7.56–7.50 (m, 3H), 7.43 (s, 1H), 7.19 (d, J = 7.8 Hz, 1H), 7.13 (d, J = 8.5 Hz, 2H), 6.95 (d, J = 8.4 Hz, 2H), 5.92 (d, J = 2.2 Hz, 1H), 5.88 (d, J = 8.3 Hz, 1H), 5.81 (d, J = 2.3 Hz, 1H), 3.00 (s, 2H), 2.28 (br, 11H), 1.91 (s, 3H). HRMS (ESI) for $C_{33}H_{33}N_5O_3$ $[M + H]^+$, calcd: 548.2656, found: 548.2651.

*4.1.5. General procedure for preparation of compounds **9** and **10**.*

A mixture of compound **8** (0.6 mmol), TBTU (0.72 mmol), HOBT (0.72 mmol), DIPEA, and appropriate amine (0.9 mmol) in DMF was stirred for 5 h at room temperature. The mixture was poured into water, and stirred for 0.5 h. The precipitate was filtered off to give a crude product, which was purified by column chromatography (CH_2Cl_2/MeOH, 100/1 to 10/1) to give the desired compound.

*4.1.5.1. (Z)-N-methyl-3-(((4-(2-methyl-5-((4-methylpiperazin-1-yl)methyl)-1H-pyrrol-1-yl)phenyl)amino)(phenyl)methylene)-2-oxoindoline-6-carboxamide (**9**).* Yellow solid. Yield: 46%. Mp: 230.7–234.0 °C. ^{1}H NMR (600 MHz, DMSO-d_6) δ 12.13 (s, 1H), 10.95 (s, 1H), 8.19 (m, J = 4.4 Hz, 1H), 7.62–7.55 (m, 3H), 7.54–7.50 (m, 2H), 7.36 (s, 1H), 7.12 (d, J = 8.7 Hz, 2H), 7.07 (s, 1H), 6.92 (d, J = 8.7 Hz, 2H), 5.88 (d, J = 3.2 Hz, 1H), 5.80 (t, J = 6.0 Hz, 2H), 2.95 (s, 2H), 2.72 (d, J = 4.5 Hz, 3H), 2.11 (br, 11H), 1.91 (s, 3H). HRMS (ESI) for $C_{34}H_{36}N_6O_2$ $[M + H]^+$, calcd: 561.2973, found: 561.2976.

4.1.5.2.

*(Z)-N,N-dimethyl-3-(((4-(2-methyl-5-((4-methylpiperazin-1-yl)methyl)-1H-pyrrol-1-yl)phenyl)amino)(phenyl)methylene)-2-oxoindoline-6-carboxamide (**10**).* Yellow solid. Yield: 46%. Mp: 221.4–223.6 °C. ^{1}H NMR (600 MHz, DMSO-d_6) δ 12.12 (s, 1H), 10.87 (s, 1H), 7.60–7.55 (m, 3H), 7.52 (d, J = 6.8 Hz, 2H), 7.11 (d, J = 8.6 Hz, 2H), 6.91 (s, 1H), 6.89 (d, J = 4.3 Hz, 2H), 6.63 (dd, J = 8.0, 1.3 Hz, 1H), 5.88 (d, J = 3.2 Hz, 1H), 5.84 (d, J = 8.0 Hz, 1H), 5.79 (d, J = 2.8 Hz, 1H), 2.95 (s, 2H), 2.90 (s, 6H), 2.14 (br, 11H), 1.91 (s, 3H). HRMS (ESI) for $C_{35}H_{38}N_6O_2$ $[M + H]^+$, calcd: 575.3129, found: 575.3122.

4.2. Pharmacology

4.2.1. Enzyme activity assay

The activities of compounds in inhibition of selected kinases were tested by Shanghai ChemPartner Co., Ltd using a well-established mobility shift assay. Details of the experiment have been described in reference.[17,18]

4.2.2. Western blotting analysis

HT-29 and HepG2 cells were cultured in 6-well plate over night and treated with **7h** for 24h. About 1×10^6 cells were collected for immuno blotting analysis. The primary antibody p-ERK, ERK, p-AKT, AKT (all from Cell Signaling Technology), GAPDH (HangZhou GoodHere Technology), and secondary antibody were used. The bands were visualized with chemiluminescence (ECL or Dura; Thermo Scientific). Representative blots are shown from several experiments. Exposure analysis of immunoblot strip was conducted by Gel imaging instrument (ChemiDoc XRS+, Bio-Rad).

4.2.3. Colony formation assay

HT-29, MKN74, and HepG2 cancer cells were treated with **7h** or nintedanib for 14 days. Details of the experiment have been described in reference.[22]

4.2.4. Flow cytometric assay

HUVECs were treated with different concentrations of compound **7h** for 48 hours, while HT-29, MKN74, and HepG2 cells were treated for 72 hours, respectively. Details of the experiment have been described in reference.[22]

4.2.5. In vitro metabolic stability assay

In vitro metabolic stability assay of compound **7h** being incubated with human and mouse liver microsomes was performed by Shanghai ChemPartner Co., Ltd. More experiment details could be seen http://www.shangpharma.com/dmpk-2/.

4.2.6. Mouse tumor xenograft efficacy study

Female nu/nu mice (4–6 weeks old) were supplied by the Experimental Animal Centre of Shenyang Pharmaceutical University and housed on particulate air-filtered ventilated racks. All procedures and treatments were conducted in accordance with the ethical regulations set by the Animal Experimentation Committee of Shenyang Pharmaceutical University.

Tumor cells at a density of 2×10^6/mL were implanted subcutaneously into the right flank of each nude mouse. When the tumor volume reached 200 mm^3, the mice were randomly assigned to control and treatment groups (n = 6 per group). The treatment groups were treated with **7h** or nintedanib via oral administration once daily.

The average tumor diameter was measured with vernier calipers twice per week. The tumor volume (TV) was calculated as follows: TV = [length (mm) × width^2 (mm^2)]/2. RTV (relative tumor volume) = $TV^{Day\ N}/TV^{Day\ 0}$ ×100%. TGI (Tumor Growth Inhibition value) = [1-RTV(treatment)/RTV(vehicle)] × 100%

4.3. Molecular docking

We used the co-crystal structure of VEGFR-2 kinase (PDB ID: 3C7Q) for the preparation of molecular docking. Water molecules and original ligand were manually removed before molecular docking. All docking calculations were performed using Autodock 4.2. For the protein, the search space was defined as a cube 30 Å on each side, centered on the protein (X, Y, Z coordinates: 21.331, 64.474, 30.745). All the other parameters used in the docking possess were set to default values. The molecular graphic manipulations and visualizations were performed using Discovery Studio Visualizer 4.0. Finally, the model with the lowest energy was used for further analysis.

Conflict of interest

The authors have declared no conflict of interest.

Acknowledgements

This work was supported by China Postdoctoral Science Foundation (2018M633720) and Liaoning Revitalization Talents Program (XLYC1808037).

References

1. Risau W. Mechanisms of angiogenesis. *Nature*. 1997;386:671–674.
2. Schenone S, Bondavalli F, Botta M. Antiangiogenic agents: an update on small molecule VEGFR inhibitors. *Curr Med Chem.* 2007;14:2495–2516.
3. Klagsbrum M, Moses MA. Molecular angiogenesis. *Chem Biol*. 1999;6:217–224.
4. Sckell A, Safabakhsh N, Dellian M, et al. Primary tumor size-dependent inhibition of angiogenesis at a secondary site: an intravital microscopic study in mice. *Cancer Res.* 1998;58:5866–5869.
5. Hanahan D, Folkman J. Patterns and emerging mechanisms of the angiogenic switch during tumourigenesis. *Cell.* 1996;86:353–364.
6. Koch S, Tugues X, Li L, et al. Signal transduction by vascular endothelial growth factor receptors. *Biochem J.* 2011;437:169–183.
7. Kowanetz M, Ferrara N. Vascular endothelial growth factor signaling pathways: therapeutic perspective. *Clin Cancer Res.* 2006;12:5018–5022.
8. Zhang Y, Chen Y, Zhang D, et al. Discovery of novel potent VEGFR-2 inhibitors exerting significant antiproliferative activity against cancer cell lines. *J Med Chem.* 2017;61:140–157.
9. Frank NY, Schatton T, Kim S, et al. VEGFR-1 expressed by malignant melanoma-initiating cells is required for tumor growth. *Cancer Res.* 2011;71:1474–1485.
10. Yang AD, Camp ER, Fan F, et al. Vascular endothelial growth factor receptor-1 activation mediates epithelial to mesenchymal transition in human pancreatic carcinoma cells. *Cancer Res.* 2006;66:46–51.
11. Su JL, Yen CJ, Chen PS, et al. The role of the VEGF-C/VEGFR-3 axis in cancer progression. *Br J Cancer.* 2007;96:541–545.

12. Andrae J, Gallini R, Betsholtz C. Role of platelet-derived growth factors in physiology and medicine. *Genes Dev.* 2008;22:1276–1312.
13. Cao Y. Multifarious functions of PDGFs and PDGFRs in tumor growth and metastasis. *Trends Mol Med.* 2013;19:460–473.
14. Roskoski R. The role of small molecule platelet-derived growth factor receptor (PDGFR) inhibitors in the treatment of neoplastic disorders. *Pharmacological Res.* 2018;129:65–83.
15. Capdevila J, Carrato A, Tabernero J, et al. What could nintedanib (BIBF 1120), a triple inhibitor of VEGFR, PDGFR, and FGFR, add to the current treatment options for patients with metastatic colorectal cancer? *Crit Rev Oncol hemat.* 2014;92:83–106.
16. Hilberg F, Roth GJ, Krssak M, et al. BIBF 1120: triple angiokinase inhibitor with sustained receptor blockade and good antitumor efficacy. *Cancer Res.* 2008;68:4774–4782.
17. Qin M, Tian Y, Sun X, et al. Novel methyl indolinone-6-carboxylates containing an indole moiety as angiokinase inhibitors. *Eur J Med Chem.* 2017;139:492–502.
18. Qin M, Yan S, Wang L, et al. Novel 6-methoxycarbonyl indolinones bearing a pyrrole Mannich base moiety as angiokinase inhibitors. *Bioorg Med Chem.* 2017;25:1778–1786.
19. Reck M. Nintedanib: examining the development and mechanism of action of a novel triple angiokinase inhibitor. *Expert Rev Anticancer Ther.* 2015;15:579–594.
20. Kharkar PS. Cancer stem cell (CSC) inhibitors: a review of recent patents (2012-2015). *Expert Opin Ther Pat.* 2017;27:753–761.
21. Curtin JA, Busam K, Pinkel D, et al. Somatic activation of KIT in distinct subtypes of melanoma. *J Clin Oncol.* 2006;24:4340–4346.
22. Ye W, Yao Q, Yu S, et al. Synthesis and antitumor activity of triazole-containing sorafenib analogs. *Molecules.* 2017;22:1759–1770.